# A SANS Contrast Variation Study of Microemulsion Droplet Growth

**Joakim Balogh,*,† Ulf Olsson,† and Jan Skov Pedersen‡**

*Physical Chemistry 1, Center for Chemistry and Chemical Engineering, Lund University, P.O. Box 125, SE-221 00 Lund, Sweden, and Department of Chemistry and iNANO Interdisciplinary Nanoscience Center, University of Aarhus, DK-8000 Aarhus C, Denmark*

*Received: September 14, 2006; In Final Form: November 15, 2006*

An extensive small angle neutron scattering study is presented using contrast variation on the growth of nonionic microemulsion droplets as the temperature and thus spontaneous curvature is varied away from the emulsification failure boundary, EFB, toward zero spontaneous curvature. Two ternary systems are compared. They only differ by the chain length of the oil (decane and hexadecane, respectively). Droplets grow in size as one moves away from the EFB. SANS data from ten different contrasts were fitted simultaneously with a model of polydisperse prolate shaped droplets interacting with an effectively hard sphere potential, and the data set further included three different droplet concentrations and four different temperatures. The model of prolates provided a good description of the data. The prolate axial ratio, obtained from the fits, increased with increasing temperature but showed only a minor variation with the droplet concentration. The two systems with different oils behave quantitatively different. In both systems, however, the droplet growth is only minor, with maximum axial ratios of about 3−4, before a bicontinuous microemulsion is formed.

## 1. Introduction

Microemulsions are one-phase systems having substantial amounts of water and oil and where the mixture is stabilized by the addition of a suitable surfactant.[1,2] They have structure on the colloidal length scale ($10^{-9}$−$10^{-6}$ m) with water and oil domains separated by a monolayer film of surfactant molecules. There are many ways in which space can be divided into separate water and oil domains and there is hence a rich variation of microstructures in surfactant−water−oil systems. The main thermodynamic driving force for forming microemulsions comes from the preference for the surfactant to form a monolayer at the water−oil interface. However, given a certain polar/apolar interfacial area, other more subtle effects determine the preference for one structure relative to another. In our current understanding, the three most important free energy contributions are due to the curvature of the surfactant monolayers, entropies on the aggregate level, and surface forces or interaggregate interactions.

In the curvature energy model of microemulsions a very important parameter is the spontaneous curvature, $H_0$, of the surfactant monolayer.[3] Under balanced conditions, when $H_0 \approx 0$, i.e., when the film has no preference for curving toward oil or water, one typically finds a bicontinuous structure. For unbalanced conditions, when $H_0 \gg 0$ or $\ll 0$, the structure typically consists of discrete droplets of oil in water (when $H_0 \gg 0$) or water in oil ($H_0 \ll 0$). Note that we here use the convention to count curvature toward oil as positive.

The curvature energy approach has proven to be very fruitful in the attempts to understand microemulsions.[3−7] Here one focuses on the curvature elasticity of the surfactant loaded polar−apolar interface. For a given configuration, the total curvature energy is given by the surface integral of the curvature energy density, $g_c$. In a series expansion of $g_c$ one generally considers only the leading order terms, being quadratic in the curvatures, and $g_c$ is often written as[8]

$$g_c = 2\kappa(H - H_0)^2 + \bar{\kappa}K \tag{1}$$

Here, $H$ and $K$ are the mean and Gaussian curvature, respectively. $\kappa$ is the bending rigidity of the film and $\bar{\kappa}$ is the saddle splay modulus that determines the preferred topology of the film. For microemulsions this implies that for $\bar{\kappa} > 0$ a bicontinuous structure is preferred while for $\bar{\kappa} < 0$ a structure of discrete droplets is preferred.

Systems based on the nonionic surfactants $C_mH_{2m+1}(OCH_2CH_2)_nOH$ are very useful model systems for microemulsions.[3,9,10] There is no need for co-surfactants or varying salinity, as in the case of ionic surfactants, and $H_0$ can be conveniently tuned by simply varying the temperature. In this study we use the surfactant $C_{12}E_5$ for which $\kappa$ and $\bar{\kappa}$ have the values $(2.5 \pm 0.5)k_BT$ and $(-2 \pm 0.5)k_BT$, respectively, $k_B$ being the Boltzmann constant and $T$ the absolute temperature, and $H_0$ varies approximately linearly with temperature[3,10,11]

$$H_0 \approx \alpha(T - T_0) \tag{2}$$

with $\alpha \approx 5 \times 10^{-4}$ Å$^{-1}$ K$^{-1}$ from ref 11 and $T_0$ being the so-called balance temperature at which $H_0 = 0$.

The curvature energy model allows us to understand the general features of microemulsions and related phases such as lamellar and sponge phases. Also quantitative agreement can be found when comparing different phases in the phase diagram. In a study by Le et al.,[11] it was also found that a sponge phase and a droplet microemulsion could be described by using the same values of $\kappa$, $\bar{\kappa}$, and $\alpha$. However, there is still lacking a quantitative description of the microemulsion structure and phase behavior in the full range of composition and spontaneous curvature. One feature that is not fully understood is how the microemulsion droplet structure varies under constant composi-

* Address correspondence to this author. E-mail: joakim.balogh@fkem1.lu.se.
† Lund University.
‡ University of Aarhus.

10.1021/jp0660031 CCC: $37.00 
Published on Web 01/04/2007

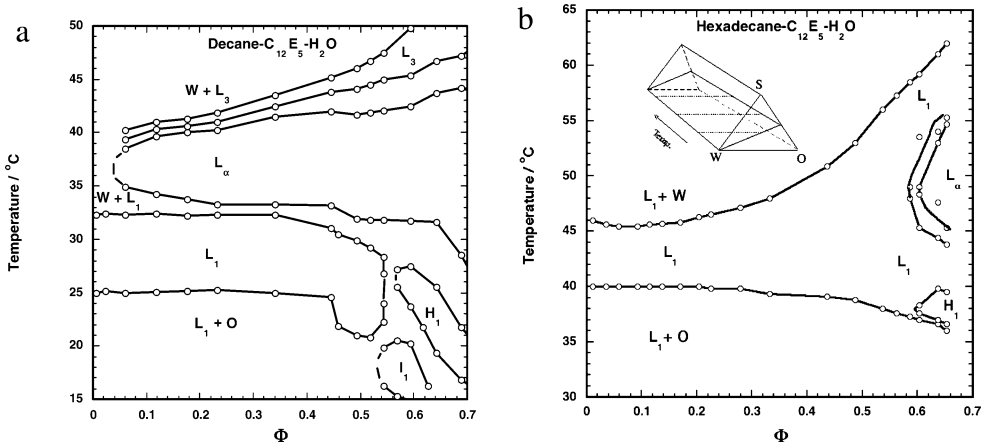


**Figure 1.** Partial phase diagram of (a) the $C_{12}E_5-H_2O$−hexadecane system and (b) the $C_{12}E_5-H_2O$−decane system, for a constant volume ratio surfactant-to-oil volume ratio of 0.815. The phase diagram is shown as temperature versus the total volume fraction of surfactant and oil. L denotes the microemulsion phase, $L_\alpha$ is a lamellar phase, and $H_1$ is a hexagonal phase. Decane data are taken from ref 11 and hexadecane data are taken from ref 15. In part b there is an illustration of the phase prism of a ternary surfactant (S)−water (W)−oil (O) system. The dashed region represents the actual cut defined by constant volume ratio surfactant-to-oil.

tion when the spontaneous curvature is varied away from the so-called emulsification failure, approaching $H_0 = 0$. Experimentally one finds that there is a growth of the droplets followed, at higher droplet concentrations, by "condensation" of the droplets into a bicontinuous structure.[12−14]

To quantify the droplet growth and droplet polydispersity we have performed an extensive small angle neutron scattering (SANS) study of two ternary microemulsion systems, only differing by the chain length of the oil. The two systems are $C_{12}E_5$−water−decane and $C_{12}E_5$−water−hexadecane. In both systems we have kept the surfactant-to-oil volume ratio constant to $\Phi_S/\Phi_O = 0.815$, $\Phi_S$ and $\Phi_O$ being the surfactant and oil volume fractions, respectively, and thus consider an oil-in-water microemulsion. By keeping this ratio constant one essentially fixes the spherical droplet radius, although the radius can be slightly different in the two systems due to a small variation in the area per $C_{12}E_5$ molecule at the interface. Partial phase diagrams of the two systems have been determined earlier[11,15] and are presented in Figure 1. The microemulsion phase, L, is stable over a temperature range of approximately 5 °C. At lower temperatures there is the so-called emulsification failure (L + O) where the microemulsion droplets coexist with an excess oil phase. At higher temperatures there is phase separation into a dilute and a concentrated microemulsion, respectively, which in the decane system but not the hexadecane system is followed by a region of lamellar phase. Another quantitative difference between the systems is that the microemulsion stability is shifted to higher temperatures in the case of hexadecane compare to decane. This difference is mainly due to a difference in $T_0$ ($T_0$ = 38 °C in the decane system and 54 °C in the hexadecane system) while the temperature coefficient $\alpha$ appears to be essentially the same.[16,17]

To maximize the information content in the SANS study we have applied contrast variation[18] by using fully deuterated oil and water with different deuterium content (mixtures of $D_2O$ and $H_2O$). The extensive data set obtained includes ten different contrasts, three different droplet concentrations, and four different temperatures in both the decane and hexadecane system, and the contrasts were chosen to cover both sides of the match point. For a given composition and temperature the data from the different contrasts were fitted simultaneously with a model of polydisperse prolate shaped droplets.

The remainder of the paper is structured as follows. First, in section 2, we describe the materials used and the details of the SANS experiments. We then, in section 3, present the model used in the analysis of the SANS data. In section 4 we present and discuss the SANS results together with fits to the data and the parameters obtained in the data analysis. Finally, in section 5, we summarize the main results and conclusions.

## 2. Materials and Methods

**Materials.** The heavy water $D_2O$ (99.8% isotopic purity) was purchased from Dr Glaser AG (Switzerland). The deuterated solvents, $C_{10}D_{22}$, (D99%) and $C_{16}D_{34}$ (D98%), were purchased from Cambridge Isotope Laboratories (Cambridge, MA). The nonionic surfactant $CH_3(CH_2)_{11}(OCH_2CH_2)_5OH$ ($C_{12}E_5$) was purchased from Nikko Chemicals (Japan). The $H_2O$ used was treated with a Millipore-Q water purification system. The other chemicals were used without further purification. When preparing the solutions with predefined volume fraction and surfactant-to-oil ratio by weighing, the following densities were used: $\rho(C_{12}E_5) = 0.967$ g/cm$^3$, $\rho$(*n*-decane-$d_{22}$) = 0.8495 g/cm$^3$, $\rho$(*n*-hexadecane-$d_{34}$) = 0.8893 g/cm$^3$, $\rho(H_2O) = 1.00$ g/cm$^3$, and $\rho(D_2O) = 1.11$ g/cm$^3$.

**Sample Preparation.** The samples were prepared by making three stock solutions: two water mixtures (corresponding to 10% of $H_2O$ in $D_2O$ and 60% of $H_2O$ in $D_2O$, respectively) and one mixture of surfactant and oil. These were then used to make 6 additional stock solutions one of each of the two water mixtures and the surfactant−oil−mixture with $\Phi = 0.10, 0.20, 0.30$. This was done to have the same volume ratio in all samples and have a controlled scattering length density. Sample compositions and contrasts are presented in Tables 1 and 2 for the decane and hexadecane systems, respectively. The samples were homogenized by mixing with a vortex mixer at approximately 5 °C above the upper stability limit of the microemulsion phase and then continuously shaken while cooling to the microemulsion phase temperature in a water bath where the homogeneous sample was stored before any measurement.

SANS Small-Angle Neutron Scattering (SANS) experiments were carried out on the SANS1 instrument at the Paul Scherrer Institut (PSI) in Villigen, Switzerland. The scattering vector modulus $q$ is defined as $q = 4\pi \sin(\theta/2)/\lambda$, where $\lambda$ is the neutron wavelength and $\theta$ is the angle between the incident and scattered neutron. The $q$ range covered was $0.0020 < q < 0.4$ Å$^{-1}$, using three instrumental configurations, all employing a mean neutron wavelength of 6 Å. The sample−detector distance

**TABLE 1: Composition of the Samples Investigated in the $C_{12}E_5$−Water−Decane System[a]**

| Φ | φ | $\rho_w$ ($10^{10}$ cm$^{-1}$) | Φ | φ | $\rho_w$ ($10^{10}$ cm$^{-1}$) |
|---|---|---|---|---|---|
| 0.343 | 0.100 | 5.69 | 0.235 | 0.373 | 3.80 |
| 0.343 | 0.204 | 4.96 | 0.235 | 0.402 | 3.59 |
| 0.343 | 0.257 | 4.60 | 0.235 | 0.447 | 3.28 |
| 0.343 | 0.293 | 4.34 | 0.235 | 0.501 | 2.91 |
| 0.343 | 0.336 | 4.05 | 0.236 | 0.600 | 2.22 |
| 0.343 | 0.375 | 3.78 | 0.119 | 0.100 | 5.69 |
| 0.343 | 0.401 | 3.60 | 0.120 | 0.204 | 4.97 |
| 0.343 | 0.451 | 3.25 | 0.120 | 0.254 | 4.62 |
| 0.343 | 0.507 | 2.87 | 0.121 | 0.300 | 4.30 |
| 0.343 | 0.600 | 2.22 | 0.121 | 0.339 | 4.03 |
| 0.233 | 0.100 | 5.69 | 0.121 | 0.381 | 3.74 |
| 0.234 | 0.206 | 4.95 | 0.121 | 0.408 | 3.55 |
| 0.234 | 0.256 | 4.60 | 0.122 | 0.454 | 3.23 |
| 0.234 | 0.305 | 4.27 | 0.122 | 0.501 | 2.90 |
| 0.234 | 0.336 | 4.05 | 0.123 | 0.600 | 2.22 |

[a] Φ is the droplet volume fraction, φ is the volume fraction of $H_2O$ in the water mixture, and $\rho_w$ is the scattering length density of the water mixture.

**TABLE 2: Composition of the Samples Investigated in the $C_{12}E_5$−Water−Hexadecane System[a]**

| Φ | φ | $\rho_w$ ($10^{10}$ cm$^{-1}$) | Φ | φ | $\rho_w$ ($10^{10}$ cm$^{-1}$) |
|---|---|---|---|---|---|
| 0.289 | 0.100 | 5.70 | 0.200 | 0.375 | 3.78 |
| 0.291 | 0.201 | 4.99 | 0.200 | 0.408 | 3.56 |
| 0.292 | 0.253 | 4.63 | 0.200 | 0.454 | 3.23 |
| 0.293 | 0.294 | 4.35 | 0.200 | 0.506 | 2.87 |
| 0.294 | 0.336 | 4.05 | 0.200 | 0.600 | 2.22 |
| 0.295 | 0.375 | 3.78 | 0.100 | 0.100 | 5.70 |
| 0.296 | 0.410 | 3.54 | 0.100 | 0.209 | 4.93 |
| 0.297 | 0.446 | 3.29 | 0.100 | 0.260 | 4.58 |
| 0.299 | 0.499 | 2.92 | 0.100 | 0.307 | 4.25 |
| 0.300 | 0.600 | 2.22 | 0.100 | 0.346 | 3.99 |
| 0.200 | 0.100 | 5.70 | 0.100 | 0.371 | 3.81 |
| 0.200 | 0.209 | 4.93 | 0.100 | 0.409 | 3.55 |
| 0.200 | 0.255 | 4.61 | 0.100 | 0.461 | 3.19 |
| 0.200 | 0.303 | 4.29 | 0.100 | 0.499 | 2.92 |
| 0.200 | 0.336 | 4.06 | 0.100 | 0.600 | 2.22 |

[a] Φ is the droplet volume fraction, φ is the volume fraction of $H_2O$ in the water mixture, and $\rho_w$ is the scattering length density of the water mixture.

of the configurations was 1.6, 6.0, and 15.0 m, respectively. The corresponding collimation lengths were 6.0, 6.0, and 15.0 m, respectively. The finite resolution of the instrument leads to smearing of the measured scattering curves.[19] This was included in the data analysis by convoluting the model curves by the instrumental resolution function.[19]

The samples were kept in quartz cells with a path length of 1.0 mm and inserted into the standard thermostated sample holder for the SANS measurements. Water was used to determine the detector sensitivity and for absolute calibration of the measured intensity, using standard procedures for the instrument.[20] This was done at 1.5 m with 6 m collimation with sufficiently good statistics and for the 6 and 15 m sample−detector distances with a shorter acquisition time so that calibration factors for both settings could be calculated. The individual cells of the 128 pixel × 128 pixel two-dimensional detector have quite uniform sensitivity. The spurious scattering around the beam stop and on the outer rim of the detector was masked. The raw data were masked, averaged, and normalized by using the BerSANS program at PSI.[21] The scattering of the empty cell beam was subtracted from the water and sample measurements with the transmission taken into account. The scattering of $D_2O$ was subtracted as background from all samples and the remaining background was accounted for by introducing a flat background in the model. This is justified since $D_2O$/$H_2O$ mixtures have a flat $q$-independent scattering. The coherent scattering component of the differential cross section per unit volume is referred to as $I(q)$ (in cm$^{-1}$).

## 3. The Fitting Model

The scattering from polydisperse spheres looks very similar to the scattering of ellipsoids, which makes it in general impossible or very difficult to separate polydispersity from particle anisotropy.[22] However, contrast variation SANS allows separation of volume/composition polydispersity and shape changes, since the former mainly influence the scattering data in the forward direction and the latter mainly influence the scattering data at higher scattering vectors. This approach has previously been used for determining the shape and polydispersity of inverse AOT microemulsion droplets[23] and it is this approach that will also be used in the present work.

To analyze the SANS on an absolute scale, a polydisperse ellipsoidal model with hard-sphere interactions was used for modeling the microemulsion droplets.[23,24] Formally the intensity can be written as

$$I(q) = \int_0^\infty n(R)\langle F(q,R)^2\rangle \, dR + \frac{1}{N}\int_0^\infty \int_0^\infty n(R)n(R')\langle F(q,R)\rangle \langle F(q,R')\rangle [S(q,R,R') - 1] \, dR \, dR' \quad (3)$$

where $n(R)$ is the size distribution, $N$ is the total number of particles, $S(q,R,R')$ are partial structure factors, and

$$\langle F(q,R)^n\rangle = \int_0^{\pi/2} F(q,R,\epsilon,\theta)^n \sin\theta \, d\theta \quad (4)$$

is the orientation averaged particle form factor. The expression (3) employs the (reasonable) approximation that orientational averages can be used for the form factor amplitudes for small degrees of shape anisotropy. The particles were taken as core−shell ellipsoids of revolution and the size was related to the neutral plane, which separate hydrophobic and hydrophilic parts of the surfactant, and given as the half axis $(R,R,\epsilon R)$, where $\epsilon \geq 1$ is the axial ratio. The form factors in eq 4 consist of a core and two layers, where the core models the oil, and the inner and outer shell model respectively the surfactant tail and head group regions. The form factors are defined in terms of the form factor of an ellipsoid[25] with constant thickness of the two shells.

Molecular constraints on volumes and areas were used extensively in the model to reduce the number of fit parameters. The volume of oil and surfactant $C_{12}$-chains (the hydrocarbon volume, $V_{hc}$) in a droplet is

$$V_{hc} = \frac{4\pi}{3}R^3\epsilon \quad (5)$$

so that the total volume fraction of oil and surfactant of $C_{12}$-chains is

$$\Phi_{hc} = \frac{4\pi}{3}\epsilon \int n(R)R^3 \, dR = \frac{4\pi}{3}\epsilon\langle R^3\rangle \quad (6)$$

where the moment of the size distribution $n(R)$ has been defined as

$$\langle R^n\rangle = \int n(R)R^n \, dR \quad (7)$$

Note that the number size distribution is normalized so that $\int n(R) \, dR = N/V$, where $N/V$ is the number density of droplets.

The total volume fractions of oil and surfactant can be calculated from the mass composition of the samples and the densities. In the present study, the surfactant-to-oil volume ratio was fixed to $\Phi_S/\Phi_O = 0.815$. The volumes of the $E_5$ and $C_{12}$ part are essentially identical. By using this, $\Phi_{hc}$ can be calculated from the mass composition of the sample and the densities. The size distribution was taken as a Gaussian in the present work. For a given value of $\epsilon$ and parameters of the size distribution ($\langle R\rangle$,$\sigma_R$), this sets the scale factor for the size distribution.

For narrow temperature ranges as investigated in the present study, the area per head group of the surfactant has been found previously to vary very little with temperature and composition (for decane[11] and for hexadecane[15]) and it is here taken as a conserved quantity. Note that this area is defined at the polar−apolar interface separating the oil and surfactant $C_{12}$-chains from water and $E_5$-groups. It should also be noted that the analysis described in this section is in fact possible without fixing the area per head group; however, the number of fit parameters is reduced by the introduction of this constraint. The fit results are essentially identical with those presented in the next section without the use of the constraints. In the analysis, the area per head group $A$ was fixed at 47 Å$^2$ throughout the fits. With a conserved surface area, the amount of surfactant in a droplet has to be scaled with surface area at the neutral plane. The total surface area of the ellipsoids is approximately[26] (valid within 1% error for $0.5 \le \epsilon \le 2$)

$$S = \frac{4\pi}{3}(2\epsilon + 1)\langle R^2\rangle \tag{8}$$

which is equal to the area $S = N_S A$ calculated from the number of $C_{12}E_5$ molecules $N_S$ and the area per head group $A$. $N_S$ is straightforwardly calculated by using the mass fraction of surfactant, the density, and the molar mass of the surfactant.

The two equations for respectively the total volume and total surface area can be used for eliminating the axial ratio $\epsilon$ from the model:

$$\epsilon = \frac{1}{\langle R^3\rangle S/\langle R^2\rangle \Phi_{hc} - 2} \tag{9}$$

Note that $S = N_S A$ and $\Phi_{hc}$, the total amount of oil and $C_{12}$-chains in the sample, are fixed at the predetermined parameters. For each of the droplets with given size $R$, the number of $C_{12}E_5$ molecules is given by $n_S = 4\pi R^2(2\epsilon + 1)/(3A)$, and since both head group volume $\upsilon_{E5}$ and $C_{12}$ volume $\upsilon_{C12}$ of the molecule are known, the $C_{12}$ volume in the droplet $V_{C12}$ is given by $V_{C12} = n_S\upsilon_{C12}$ and the $E_5$ volume $\upsilon_{E5}$ is given by $V_{E5} = n_S\upsilon_{E5}$. With this, the oil volume is $V_{oil} = V_{hc} - V_{C12}$. When water solvation of the $E_5$ head group is considered with a volume fraction $f$ of water in the $E_5$ shell, the volume of the outer shell becomes $V_{shell} = V_{E5}/(1 - f)$.

With the assumption of a constant shell thickness $\Delta_{C12}$ of the $C_{12}$ shell, the volume of $V_{C12}$ of the $C_{12}$-chains in the droplets can be expressed as

$$V_{C12} = \frac{4\pi}{3}R^3\epsilon - \frac{4\pi}{3}(R - \Delta_{C12})^2(\epsilon R - \Delta_{C12}) \tag{10}$$

and for a given radius (and $\epsilon$ value), this gives an equation for determining $\Delta_{C12}$. As $R \gg \Delta_{C12}$, the term proportional to $\Delta_{C12}^3$ can be neglected and one has a second-order polynomial for which it is easy to identify the physical meaningful positive value for $\Delta_{C12}$. Similarly, with the assumption of a constant thickness of the outer shell $\Delta_{shell}$, the volume relation for determining $\Delta_{shell}$ is

$$V_{shell} = \frac{4\pi}{3}(R + \Delta_{shell})^2(\epsilon R + \Delta_{shell}) - \frac{4\pi}{3}R^3\epsilon \tag{11}$$

where the physically meaningful value for $\Delta_{shell}$ is easily determined, when neglecting terms proportional to $\Delta_{shell}^3$.

The form factor amplitude entering eq 4 is given by

$$F(q,R,\epsilon,\theta) = \exp(-q^2\delta^2/2) \begin{bmatrix} \Delta\rho_{shell}V_{out}\Phi(qr(R,\Delta_{shell},\epsilon,\theta)) \\ -(\Delta\rho_{shell} - \Delta\rho_{C12})V_{hc}\Phi(qr(R,0,\epsilon,\theta)) \\ -(\Delta\rho_{C12} - \Delta\rho_{oil})V_{oil}\Phi(qr(R,-\Delta_{C12},\epsilon,\theta)) \end{bmatrix} \tag{12}$$

where $r(R,\Delta,\epsilon,\theta) = [(R + \Delta)^2 \sin\theta^2 + (\epsilon R + \Delta)^2 \cos\theta^2]^{1/2}$, $V_{out} = (4\pi/3)(R + \Delta_{shell})^2(\epsilon R + \Delta_{shell})$, and $\Phi(x) = \{3[\sin(x) - x\cos(x)]\}/x^3$ is the form factor amplitude of a sphere. The parameters $\Delta\rho_{shell}$, $\Delta\rho_{C12}$, and $\Delta\rho_{oil}$ are the excess scattering length densities of the shell, $C_{12}$ region, and oil, respectively. Finally, the last term $\exp(-q^2\delta^2/2)$ is a factor that gives graded interfaces of width $\delta$ between the components of the droplets. This parameter was fixed at the value 2.5 Å during the fits, which is in accordance with the previous work of Bagger-Jörgensen et al.[27]

The scattering length density of each component was calculated from the known partial specific densities and the molar mass of the molecules, using the tabulated scattering length of the constituting elements. For the $E_5$ shell, the water penetration was taken into account. Similarly the scattering length of the surrounding $H_2O-D_2O$ mixture was calculated and the excess scattering length of each component was calculated by subtracting the scattering length density of the water.

A volume fraction of the hydrated droplet can be calculated as

$$\Phi_{hydr} = \frac{4\pi}{3}\int n(R)(R + \Delta_{shell})^2(\epsilon R + \Delta_{shell})\,dR \tag{13}$$

and a volume equivalent radius can be defined by

$$R_v^3 = (R + \Delta_{shell})^2(\epsilon R + \Delta_{shell}) \tag{14}$$

The obvious first approach is to use $\Phi_{hydr}$ and $R_v$ in the structure factor calculation. However, the applied hard-sphere model assumes that the particles are strictly spherical. In fact the particles are elongated, and therefore the structure factors might not give a good description of the data. In general, the elongation means that there is not one single characteristic length scale for the particle interactions and therefore the observed structure factor effects might not be as pronounced as predicted by the model. Therefore it was decided to vary the parameters describing the interactions. The hard-sphere volume fraction $\Phi_{HS}$ of the droplets including the hydrating water was taken as a fit parameter together with a scale factor $R_{HS}/R_v$, where $R_v$ is the volume equivalent radius of the solvated volume of a droplet and $R_{HS}$ is the effective hard-sphere radius of the droplet. In the implementation used, scaling $\Phi_{HS}$ is equivalent to scaling the actual total volume fraction of the components, which is in turn used in the calculation of the absolute scattering intensity of the model. To compensate for this, it was necessary to include an overall scale factor of the model. This factor can also account for errors in absolute calibration. The product of the scale factor and the hard-sphere volume fraction should stay constant in the

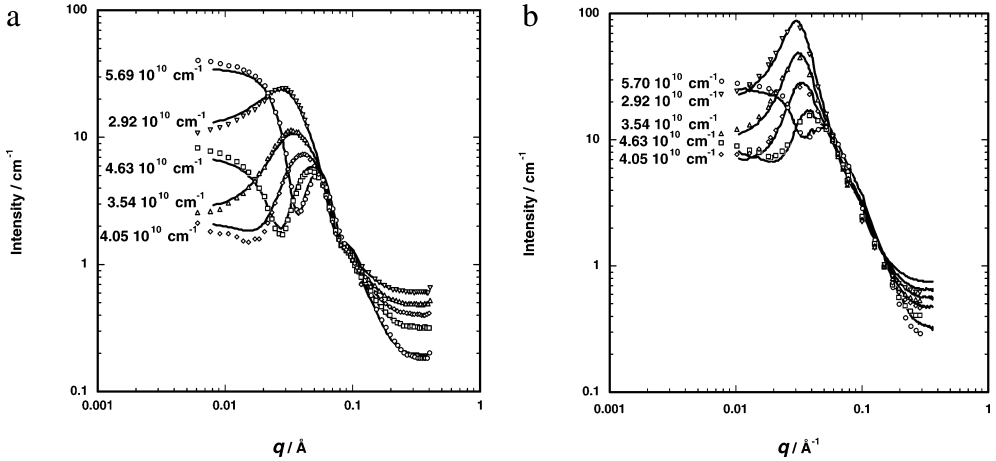


**Figure 2.** Scattered intensity versus scattering vector $q$ for some selected contrasts: (a) decane system with $\Phi = 0.12$, recorded at $T = 25$ °C, and (b) hexadecane system with $\Phi = 0.30$, recorded at $T = 40$ °C. The water scattering length densities for the different scattering curves are displayed in the figures. The continuous lines represent best fits of the model to the experimental data.

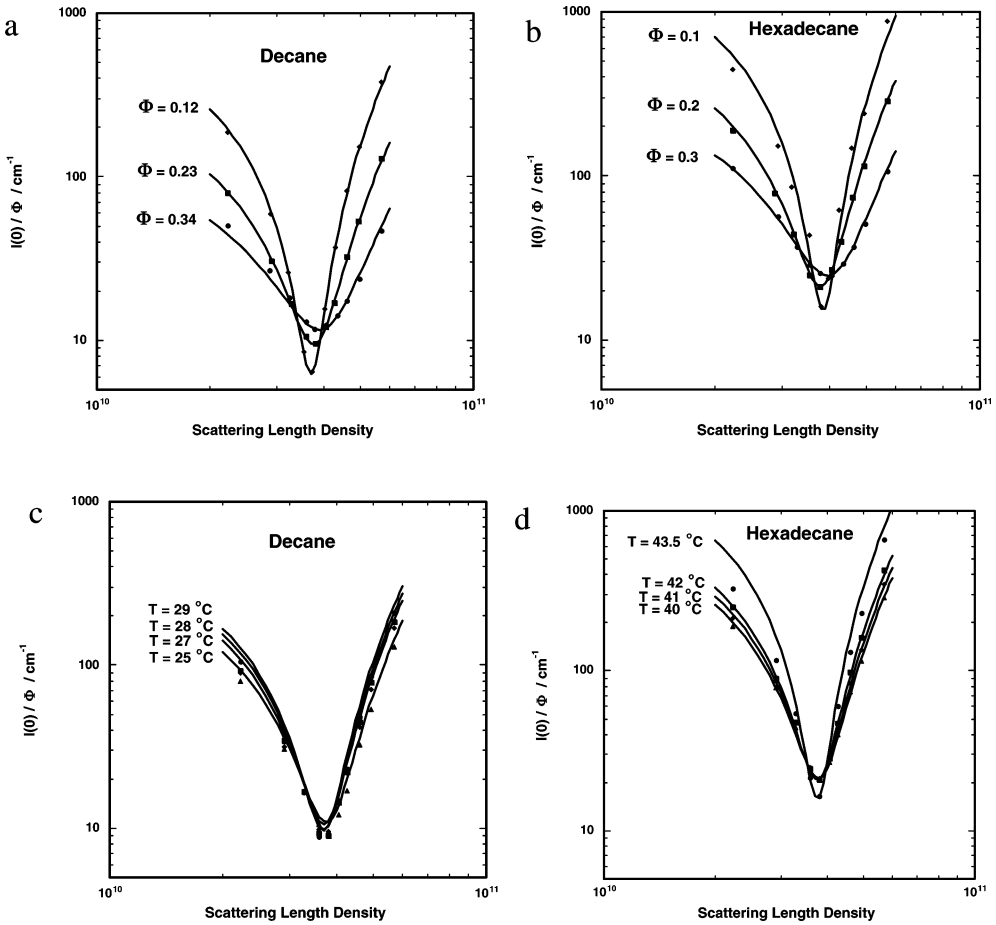


**Figure 3.** The volume fraction normalized forward scattering, $I(0)/\Phi$, as a function of the scattering length density of the water phase: (a) decane at 25 °C and different droplet concentrations, as indicated in the figure; (b) hexadecane at 40 °C and different droplet concentrations, as indicated in the figure; (c) decane system with $\Phi = 0.23$ and different temperatures as indicated in the figure; and (d) hexadecane with $\Phi = 0.10$ and different temperatures as indicated in the figure.

fits (which it did) and any deviation between the product and the hydrated volume is due to errors in absolute calibration. It was found that the absolute scale was systematically 10% lower than calculated for the model using the densities given in Section 2 above.

Note that the two parameters $\Phi_{HS}$ and $R_{HS}/R_v$ related to the structure factor effects have to be considered as effective parameters. The rotation of the droplets and shape fluctuations are expected to be faster than translational diffusion, and therefore the effective interaction potential is likely to be well-described by that of a spherically symmetric potential, however, with an interaction radius larger than the volume equivalent radius.

The data were analyzed by fitting all contrast for a certain sample simultaneously. The fit parameters $\langle R \rangle$ and $\sigma_R$ describe the size distribution. For each contrast a constant background was fitted for describing the incoherent background from the samples. To check for errors in scattering lengths, the oil

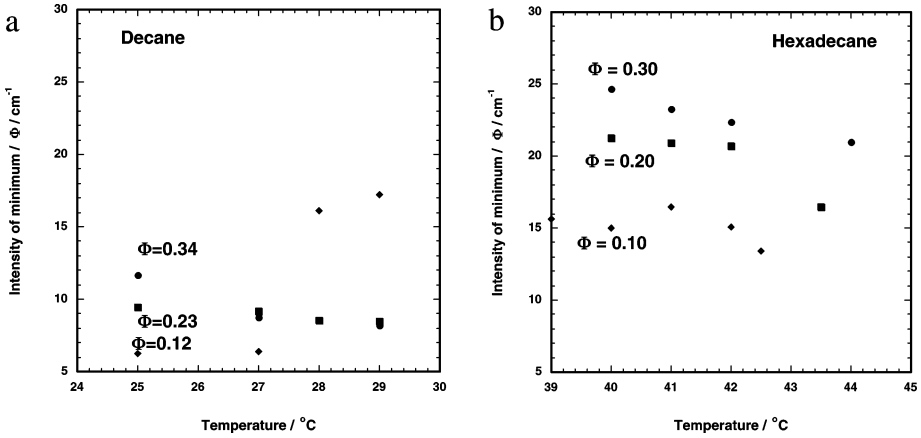


**Figure 4.** Intensity at the match point, normalized by the droplet volume fraction and plotted as a function of the temperature for the three volume fractions for decane (a) and hexadecane (b). Circles are $\Phi = 0.34$ for decane and $\Phi = 0.30$ for hexadecane, squares are $\Phi = 0.23$ for decane and $\Phi = 0.20$ for hexadecane, and diamonds are $\Phi = 0.12$ for decane and $\Phi = 0.10$ for hexadecane.

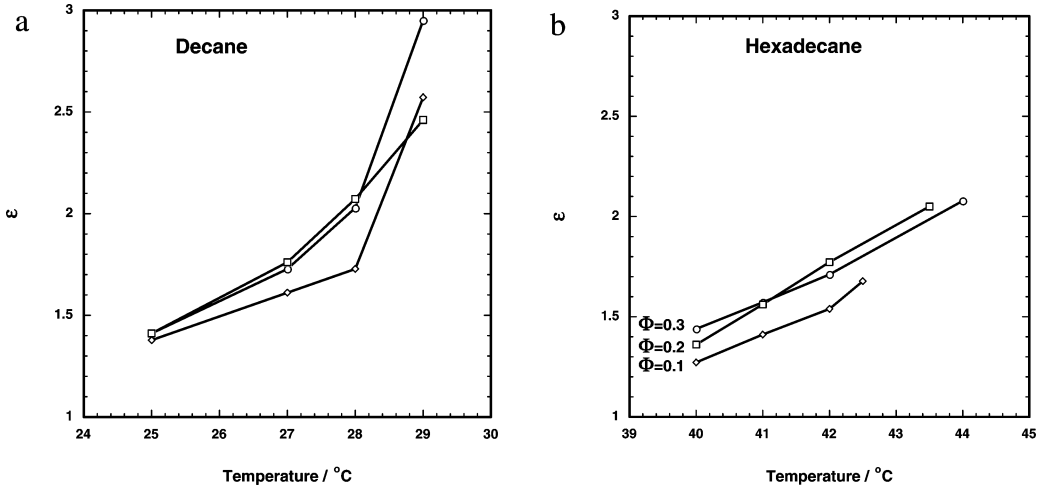


**Figure 5.** (a) The axial ratio (eccentricity) plotted versus temperature for the decane system at different droplet volume fractions. Circles represent $\Phi = 0.34$, squares $\Phi = 0.23$, and diamonds $\Phi = 0.12$. (b) The axial ratio (eccentricity) plotted versus temperature for the hexadecane system at different droplet volume fractions. Circles represent $\Phi = 0.30$, squares $\Phi = 0.20$, and diamonds $\Phi = 0.10$.

scattering length density was treated as a global fit parameter; however, it turned out that the final values deviated only a few percent from the calculated ones. Note that adjustment of this parameter makes it possible to adjust the match point of the model.

## 4. Results and Discussion

A total of 720 measurements resulting in 720 scattering curves have been done. This high number comes from ten scattering length densities, four temperatures, two oils, three volume ratios, and three detector distances ($q$ ranges). Due to the large number of data sets measured, only a small subset is displayed in the present paper. Figure 2 shows a full contrast variation data set for both decane and hexadecane, for temperatures of respectively 27 and 42 °C and a volume fraction of 0.3. A very large variation of the shape of the curves with contrast is observed. It has previously been shown by model calculations[23] that contrast dependence of the forward scattering ($q = 0$) contains information on, e.g., composition polydispersity of the droplets in the microemulsion. Therefore the volume fraction normalized $I(q=0)/\Phi$ was derived from the data and plotted as a function of the scattering length density of the water phase. Data for a constant temperature and for different volume fractions are shown in Figure 3a,b. The minimum is deeper, the lower the volume fraction. This is due to a smaller spread in match point and it thus indicates that the composition polydispersity is decreasing for decreasing volume fraction. The interference effects due to the finite concentrations disappear at the match points, but become significant as one moves away from the match point. Therefore, far away from the match point, the values of $I(0)/\Phi$ decrease with increasing volume fraction.

Panels b and d of Figure 3 show the data for respectively decane and hexadecane, at constant volume fraction at different temperatures. The variation with temperature is quite small, and it can be concluded that the variation in composition polydispersity is very small. Away from the match point, the $I(0)$ increases with increasing temperature. This is due to the growth of the droplets with increasing temperature, as will be discussed further below.

The next step in the analysis was to employ the advanced model described in the previous section for fitting each contrast variation series simultaneously. The curves in Figure 2 are the fits for prolate ellipsoids. As can be seen, a very good agreement between model and data is obtained. Similar good fits were obtained for all the compositions and temperatures. The only parameter, which for a fixed volume fraction displays a large variation as a function of temperature, is the axial ratio $\epsilon$. This parameter is displayed in Figure 5a for decane, and in Figure 5b for hexadecane. Close to the lower phase boundary, at the lowest temperature in the figures, the droplets are only slightly

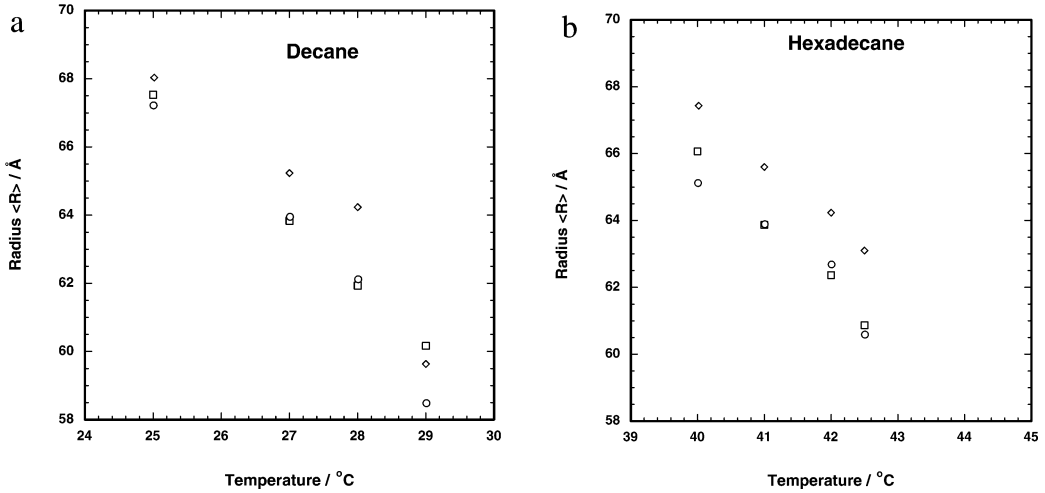


**Figure 6.** (a) The average radius $\langle R \rangle$ of the short axis of the droplets as a function of temperature for the decane system at different droplet volume fractions. Circles represent $\Phi = 0.34$, squares $\Phi = 0.23$ and diamonds $\Phi = 0.12$. (b). The average radius $\langle R \rangle$ of the short axis of the droplets as a function of temperature for the hexadecane system at different droplet volume fractions. Circles represent $\Phi = 0.30$, squares $\Phi = 0.20$, and diamonds $\Phi = 0.10$.

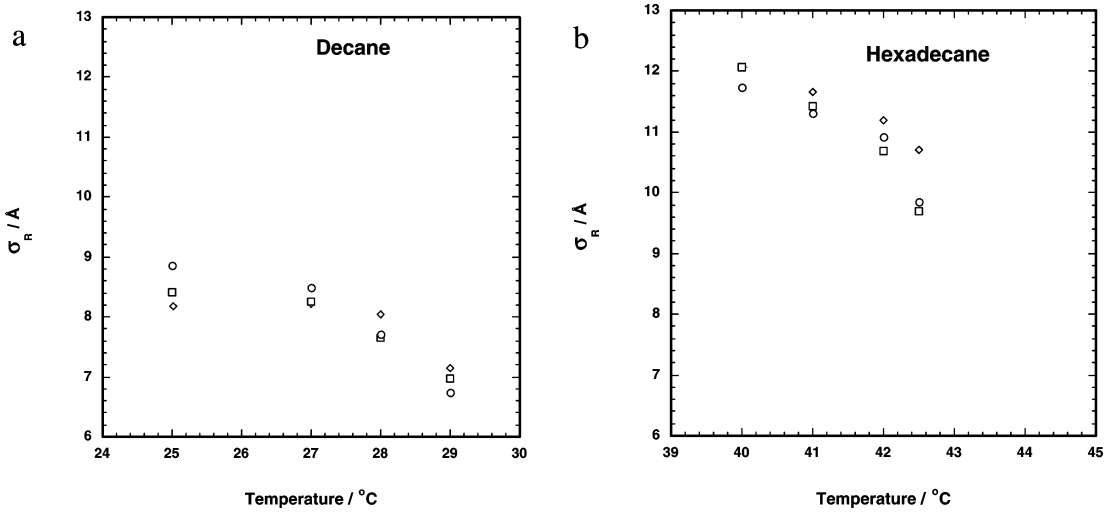


**Figure 7.** (a) Polydispersity of the radius $\sigma_R$ as a function of temperature for the decane system at different droplet volume fractions. Circles represent $\Phi = 0.34$, squares $\Phi = 0.23$, and diamonds $\Phi = 0.12$. (b). Polydispersity of the radius $\sigma_R$ as a function of temperature for the hexadecane system at different droplet volume fractions. Circles represent $\Phi = 0.30$, squares $\Phi = 0.20$, and diamonds $\Phi = 0.10$.

elongated with $\epsilon \approx 1.3-1.4$ for both decane and hexadecane. The droplets increase in length to about $\epsilon \approx 1.8$ when increasing the temperature by about 3 deg. Upon further increase, the droplets with decane have a pronounced increase to $\epsilon \approx 2.5-3$ at 4 deg above the lower phase boundary. The droplets with hexadecane increase less to $\epsilon \approx 2$ for $\Phi = 0.20$ and 0.3 at 3.5−4 deg above the lower phase boundary; for $\Phi = 0.10$, data are not available at such high temperatures. Similar ranges of $\epsilon$ values have been found from analyzing $^2$H NMR relaxation data.[15,28] However, in the NMR study, $\epsilon$ was found to increase both with temperature and with concentration, at least at higher temperatures. In fact, for nonspherical droplets, one does expect the droplets to grow in size with increasing concentration as the relative impact of the entropy of mixing decreases. This discrepancy needs to be further investigated.

The average radius $\langle R \rangle$ of the short axis of the droplets is shown in Figure 6. As a function of the temperature separation from the lower phase boundary, the temperature dependence is almost identical for decane and hexadecane. In both cases, it decreases with increasing temperature. The increase in axial ratio (i.e., the growth of the droplet length) is coupled to this decrease through the conservation of head group area. The polydispersity of the radius $\sigma_R$ is shown in Figure 7. It is significantly smaller for decane than for hexadecane. The deviation is ascribed to the difference in temperature of the two sets of measurements. The higher temperature of the hexadecane samples leads to more fluctuations in sample composition and thus to higher polydispersity. For both oils, the polydispersity decreases with temperature. This is a consequence of the fluctuations being more limited as the smaller axis radius of the droplets decreases.

The hard-sphere volume fractions for decane are $\Phi_{HS} = 0.32-0.42$ for $\Phi = 0.34$, $\Phi_{HS} = 0.21-0.22$ for $\Phi = 0.23$, and $\Phi_{HS} = 0.07-0.09$ for $\Phi = 0.12$. So in this case, there is a reasonable agreement between the hard-sphere volume fractions and the actual nonhydrated volume fraction of oil and surfactant. However, for the lowest volume fraction $\Phi_{HS}$ is significantly lower than $\Phi$. For hexadecane $\Phi_{HS} \approx 0.23$ for $\Phi = 0.30$, $\Phi_{HS} \approx 0.14-0.15$ for $\Phi = 0.20$, and $\Phi_{HS} \approx 0.07$ for $\Phi = 0.10$. So for hexadecane $\Phi_{HS}$ is significantly lower than $\Phi$ for all three volume fractions. The solvent quality of water for poly(ethylene oxide) decreases significantly with temperature. Therefore the repulsion between the droplets is lower for hexadecane than for decane and this leads to a lower hard-sphere volume fraction in the latter case.

The ratio between the hard-sphere interaction radius and the volume equivalent radius $R_{HS}/R_v$ is quite constant and lies in the range 0.93−1.04 for decane. For hexadecane, it varies in the range 0.93−1.08 with a clear tendency of a decrease in the value with temperature. The small variation of $R_{HS}/R_v$ suggests that the droplets interact effectively as spherical objects with an interaction radius given by the volume. This is in good agreement with the previously given arguments for applying the model to the present systems.

## 5. Summary and Conclusions

We have studied the growth of nonionic microemulsion droplets with temperature using an extensive contrast variation SANS study. Two systems were investigated and compared, only differing by the chain length of the oil (decane and hexadecane, respectively). The droplets were modeled as polydisperse prolates interacting through an effective hard-sphere potential. From the data analysis we find a moderate growth of the droplets with increasing temperature with axial ratios reaching 2−3 at the onset of formation of a bicontinuous network. A similar droplet growth was found in the two systems although with minor quantitative differences. The hexadecane system has a slightly higher polydispersity, which is consistent with the fact that the temperature was higher in those experiments. However, the temperature difference is not very large (5% in K) so the results also indicate that the bending rigidity is smaller in the hexadecane system. The moderate droplet growth found here is consistent with previous findings. The reason for only a moderate growth is the penalty from the entropy of mixing of the droplets. Also the smallest possible droplet having a spherical shape still is quite large and we have a low number density of droplets.

When comparing results from different methods it is important to have in mind that, e.g., the axial ratio obtained from the analysis is model dependent. The model is often a significant simplification compared to reality to keep the number of variables to a number that one is able to handle. Thus, we have for example in the present model introduced constraints regarding the shape and we have considered only size polydispersity and not shape polydispersity. We note also that the spontaneous curvature depends on the $H_2O/D_2O$ ratio due to slightly different solvations of the $E_5$-chains. Replacing $H_2O$ with $D_2O$ appears to have the same effect as lowering the temperature by approximately 1.5−2 °C.[29] Thus when we vary the $H_2O$-to-$D_2O$ ratio in our contrast variation experiment we vary the spontaneous curvature by the amount corresponding to a temperature shift of 1 °C across the sample series, adding some uncertainty in the analyzed parameters. However, the effect is relatively small, and we can in practice consider the contrast variation data sets as being consistent.

At the match point we obtain from the finite forward scattering a measure of the composition polydispersity, i.e., the fluctuation of $\Phi_S/\Phi_O$ around the mean value 0.815. The width of this fluctuation does not seem to vary significantly with the temperature, which is an interesting observation, in view of the fact that the number density of droplets reduces to about a half.

The general problem of shape and size of microemulsion droplets is complicated, including the problem of how to count the entropy in concentrated polydisperse systems of nonspherical droplets. A general approach involving writing the droplet interface in a series of spherical harmonics has been used,[30−32] where equipartition is assumed to govern the relative amplitudes of the shape fluctuation modes. We hope to return to this problem in a future publication.

**Acknowledgment.** This work was financially supported by the Swedish Foundation for Strategic Research (SSF) through the Colloid and Interface Technology Programme. U.O. thanks the Swedish Research Council (V.R.) for financial support. J.S.P thanks the Danish Natural Science Research Council for financial support. This work is based on experiments performed at the Swiss spallation neutron source SINQ, Paul Scherrer Institut, Villingen, Switzerland. This research project has been supported by European Commission under the 6th Framework Programme through the Key Action: Strengthening the European Research Area, Research Infrastructures, Contract No. RII−CT-2003-505925. We are grateful for the help from Joachim Kolbrecher and Steven van Petegem during our stays at PSI.

## References and Notes

(1) Evans, D. F.; Wennerström, H. *The Colloidal domain*: *where physics, chemistry, biology and technology meet*, 2nd ed.; John Wiley & Sons, Inc: New York, 1999.
(2) Holmberg, K. *Handbook of Applied Surface and Colloid Chemistry*; John Wiley & Sons Ltd: Chichester, UK, 2002; Vol. 1.
(3) Olsson, U.; Wennerström, H. *Adv. Colloid Interface Sci.* **1994**, *49*, 113−146.
(4) Daicic, J.; Olsson, U.; Wennerström, H. *Langmuir* **1995**, *11*, 2451−2458.
(5) Gompper, G.; Schick, M. *Phase Transitions and Critical Phenomena*; Academic Press: London, UK, 1994; Vol. 16.
(6) Safran, S. A. In *Structures and Dynamics of Strongly Interacting Colloids and Supramolecular Aggregates in Solution*; Chen, S., Huang, J. S., Tartaglia, P., Eds.; Kluwer Academic Publishers: Dordrecht, The Netherlands, 1992; p 237.
(7) Safran, S. A. *Adv. Phys.* **1999**, *48*, 395−448.
(8) Helfrich, W. *Z. Naturforsch.* **1973**, *28c*, 693−703.
(9) Kahlweit, M.; Strey, R. *Angew. Chem., Int Ed.* **1985**, *24*, 654−668.
(10) Strey, R. *Colloid Polym. Sci.* **1994**, *272*, 1005−1019.
(11) Le, T. D.; Olsson, U.; Wennerström, H.; Schurtenberger, P. *Phys. Rev. E* **1999**, *60*, 4300−4309.
(12) Olsson, U.; Nagai, K.; Wennerström, H. *J. Phys. Chem.* **1988**, *92*, 6675−6679.
(13) Leaver, M. S.; Olsson, U.; Wennerström, H.; Strey, R. *J. Phys. II* **1994**, *4*, 515−531.
(14) Leaver, M.; Furo, I.; Olsson, U. *Langmuir* **1995**, *11*, 1524−1529.
(15) Balogh, J.; Olsson, U.; Pedersen, J. S. *J. Dispersion Sci. Technol.* **2006**, *27*, 497−510.
(16) Balogh, J.; Kaper, H.; Olsson, U.; Wennerström, H. *Phys. Rev. E* **2006**, *73*, 041506.
(17) Sottmann, T.; Strey, R. *J. Chem. Phys.* **1997**, *106*, 8606−8615.
(18) Schurtenberger, P. In *Neutones, X-rays and lightscattering Applied to Soft Condensed Matter*; Lindner, P., Zemb, T., Eds.; North-Holland: Amsterdam, The Netherlands, 2002; p 145.
(19) Pedersen, J. S.; Posselt, D.; Mortensen, K. *J. Appl. Crystallogr.* **1990**, *23*, 321−333.
(20) Kohlbrecher, J.; Wagner, W. *J. Appl. Crystallogr.* **2000**, *33*, 804−806.
(21) Keiderling, U. *Appl. Phys. A: Mater. Sci. Process.* **2002**, *74*, s1455−s1457.
(22) Caponetti, E.; Floriano, M. A.; Didio, E.; Triolo, R. *J. Appl. Crystallogr.* **1993**, *26*, 612−615.
(23) Arleth, L.; Pedersen, J. S. *Phys. Rev. E* **2001**, *63*, 061406.
(24) Vrij, A. *J. Chem. Phys.* **1979**, *71*, 3267−3270.
(25) Guinier, A. *Ann. Phys.* **1939**, *12*, 161.
(26) Pedersen, J. S. Unpublished.
(27) Bagger-Jörgensen, H.; Olsson, U.; Mortensen, K. *Langmuir* **1997**, *13*, 1413−1421.
(28) Balogh, J.; Olsson, U. *J. Dispersion Sci. Technol.* **2007**, in press.
(29) Strey, R.; Schomäcker, R.; Roux, D.; Nallet, F.; Olsson, U. *J. Chem. Soc., Faraday Trans.* **1990**, *86*, 2253−2261.
(30) Safran, S. A. *J. Chem. Phys.* **1983**, *78*, 2073−2076.
(31) Milner, S. T.; Safran, S. A. *Phys. Rev. A* **1987**, *36*, 4371−4379.
(32) Gradzielski, M.; Langevin, D.; Farago, B. *Phys. Rev. E* **1996**, *53*, 3900−3919.